Toward an Intercalibrated Fundamental Climate Data Record of the SSM/I Sensors

Mathew R. P. Sapiano, Wesley K. Berg, Darren S. McKague, and Christian D. Kummerow

***Abstract*—Multiple independent intercalibration techniques are used to derive calibration adjustments for the development of a fundamental climate data record of physically consistent brightness temperature data from the series of six *special sensor microwave/imagers* (SSM/Is). The techniques include direct polar matchups, double differencing against model simulations from reanalysis profile data, double differencing against matchups with the Tropical Rainfall Measuring Mission Microwave Imager, vicarious cold calibration, and an Amazon warm calibration. Multiple realizations of three of the five techniques have been applied using different reanalysis data and retrieval techniques to account for Earth incidence angle-dependent differences between sensors. Excellent agreement has been achieved between each of the techniques with typical spread within 0.5 K at the cold end, with slightly higher spread when the warm end estimate is included. A strategy for estimating mean intercalibration values is described with justification for the use of a simple offset based on error characteristics. Intercalibration offsets are smaller for the more recent SSM/I ($<$ 1 K for F14 and F15 compared with F13) and slightly larger for the older satellites ($<$ 2 K for F08, F10, and F11 when compared to F13).**

***Index Terms*—Climate data record, intercalibration, passive microwave remote sensing, special sensor microwave/imagers (SSM/I).**

I. Introduction

THE SPECIAL Sensor Microwave/Imager (SSM/I) [1] is a conically scanning seven-channel microwave radiometer flown aboard the Defense Meteorological Satellite Program (DMSP) sun-synchronous satellites from 1987 to the present. Retrievals from the SSM/I instrument have been used for a vast array of applications in both operational meteorology and climatology. Commonly derived parameters include precipitation, ocean wind speed, water vapor, cloud liquid water and ice cover, age, and concentration. The SSMI record is particularly important for climate studies that require a homogeneous record. The six SSM/I instruments span a total period of 25 years (the SSM/I flying aboard F15 is still operational, but with degraded capacity) and have the same architecture, thus reducing differences caused by sensor design differences. While such differences are expected to be small between SSM/I instruments, the calibration of the six instruments is by no means identical, and so intercalibration is required to ensure consistency of the brightness temperature (Tb) data record for climate applications.

The SSM/I has four frequencies (19.35, 22.235, 37.0, and 85.5 GHz) each of which has both vertically and horizontally polarized channels, with the exception of the 22 GHz that has only vertical polarization. The sampling of the SSM/I is such that the 19, 22, and 37-GHz (low-resolution) channels have a sampling interval of $\sim$25 km and a swath width of 1400 km. The 85-GHz (high-resolution) channels have twice the number of along track and across track samples with a sampling interval of $\sim$12.5 km. With the exception of the poles, complete earth coverage is achieved every 2–3 days. Several important failures occurred to SSM/I sensors that require special handling and correction. The F08 SSM/I suffered a failure of the 85-GHZ v-pol channel in early 1989 with the h-pol channel failing in early 1991. Additionally, there are no data for most of December 1987. In August 2006, interference from a beacon onboard F15 led to the introduction of significant noise in the 22-GHz channel. Corrections for this noise have been developed [2], but the interference is not sufficiently stable for climate purposes and the F15 data are unsuitable for intercalibration purposes from August 2006 onward.

The main goal of this work is to intercalibrate the six SSM/I sensors to a common calibration standard for use in developing climate data records (CDRs). It is important to note that intercalibration does not imply that the derived correction will completely homogenize observations from the sensor. Instead, the intercalibration procedure must ensure that measurements between the sensors are physically consistent. In addition to calibration errors, observations from the SSM/I sensors can differ due to several physical mechanisms including diurnal sampling differences and view angle or Earth incidence angle (EIA) differences. In the case of the SSM/I, the channel and instrument differences are expected to be negligible, although differences could exist due to fabrication variations/errors since the six sensors were not all built at the same time. In contrast, differences in diurnal sampling and EIA both vary across SSM/I instruments and must be properly accounted for in order to accurately intercalibrate the sensors.

Fig. 1(a) shows the local equator crossing time of the DMSP satellites that carried the SSM/I, and Fig. 1(b) shows the mean

Manuscript received January 31, 2012; revised May 22, 2012; accepted June 2, 2012. Date of publication July 30, 2012; date of current version February 21, 2013. This work was supported by the National Oceanic and Atmospheric Administration under Grant NA09OAR4320893#9.

M. R. P. Sapiano is with Earth Systems Science Interdisciplinary Center, University of Maryland, College Park, MD 20740-3823 USA (e-mail: msapiano@umd.edu).

W. K. Berg and C. D. Kummerow are with the Department of Atmospheric Science, Colorado State University, Fort Collins, CO 80523 USA (e-mail: berg@atmos.colostate.edu; kummerow@atmos.colostate.edu).

D. S. McKague is with Atmospheric, Oceanic and Space Sciences, University of Michigan, Ann Arbor, MI 48109-2143 USA (e-mail: dmckague@umich.edu).

Color versions of one or more of the figures in this paper are available online at http://ieeexplore.ieee.org.

Digital Object Identifier 10.1109/TGRS.2012.2206601

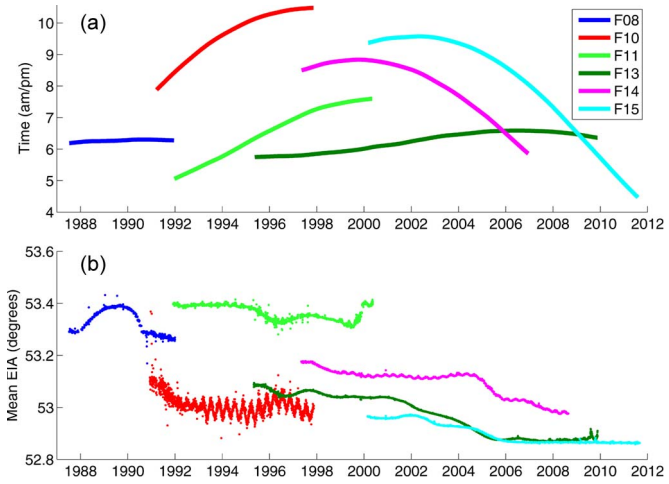

Fig. 1. Time series of (a) local equator crossing time and (b) mean Earth incidence angle for each of the SSM/I instruments.

EIA of each of the SSM/I as calculated by Berg *et al.* [3]. The sun-synchronous DMSP satellites were launched into orbits with local observing times around 6 A.M./P.M. and 8 A.M./P.M., although significant drift occurred particularly after the main operational segment of the satellites lifetime. Differences due to diurnal sampling can lead to large differences in the observed Tb due to aliasing with the diurnal cycle of weather (particularly clouds). As shown in Fig. 1(b), differences in the respective EIAs between SSM/I sensors are also comparatively large with some changes over time. Berg *et al.* [3] estimated that a half-degree EIA difference can be associated with as much as a 1 K Tb difference in the v-pol channels. While the impact of this difference on weather applications would be relatively small, such differences can be critical on the climate scale, and so the intercalibration must properly account for EIA differences between sensors and the EIA must be properly accounted for in geophysical retrievals.

Several studies have applied different techniques to estimate intercalibration for the SSM/I Tb. Wentz [4] used crossovers from a one-year period to intercalibrate the SSM/I to a calibrated version of F08. Yang *et al.* [5] used a similar polar overpass technique to compare Tb for matched footprints within 3 km and two minutes of each other. Colton and Poe [6] used comparisons of monthly mean Tb and histograms of annual Tb to evaluate differences between sensors. Andersson *et al.* [7] used a linear regression of matched, rain-free 1°, ten-day average SSM/I Tb that were adjusted to a common EIA. In addition to these studies where Tb are intercalibrated, many more studies have intercalibrated derived geophysical parameters (e.g., [8] and [9]) although this approach is not applicable for this study. In addition, several studies have intercalibrated SSMIS [10] with SSM/I (e.g., [11]).

Perhaps the largest issue with the intercalibration techniques applied thus far for SSM/I is the lack of multiple corroborating approaches. All of these studies use a single technique, and it has been difficult to isolate sources of disagreement, particularly when varying screening and averaging is used and when the absolute calibration is different and unknown. The goal of the present study is to apply multiple intercalibration techniques to a common, quality-controlled data set with accurately known EIA information and common screening/averaging procedures. The use of multiple techniques gives an estimate of the technique-dependent error, which is a highly useful measure and provides a more objective estimate of the residual uncertainty than the error estimates from individual techniques. At a more basic level, agreement between several largely independent techniques helps lend significant confidence in the resulting intercalibration.

TABLE I
DETAILS FOR SSM/I SENSORS

DMSP satellite	Launch date	FCDR record dates		Notes
		Start	End	
F08	Jun 20, 1987	Jul 1987	Dec 1991	Dec 1987: no data; 85V failed: Jan 1989; 85H failed: Feb 1991
F10	Dec 1, 1990	Dec 1990	Nov 1997	
F11	Nov 28, 1991	Feb 1992	May 2000	Limited sampling in 1997
F13	Mar 24, 1995	May 1995	Nov 2009	
F14	Apr 4, 1997	May 1997	Aug 2008	
F15	Dec 12, 1999	Feb 2000	Present (used up to Jul 2006)	RADCAL beacon interference in 22V starting Jul 2006

II. SSM/I DATA

The SSM/I data used for this study were collected as part of a National Oceanic and Atmospheric Administration-funded project to create a fundamental CDR (FCDR) of intercalibrated Tb from the series of microwave imagers on board the DMSP satellites. This analysis focuses only on the series of six SSM/I sensors, which operated from July 1987 through November 2009. Table I contains the launch dates for the six SSM/I sensors as well as the dates for which data exist in the FCDR. Before an analysis of intercalibration differences could be undertaken, however, a number of processing steps had to be developed and/or applied. First, the original temperature data records (TDRs) files were reformatted into NetCDF4 and broken into single orbit granules. Duplicate scans were removed, and quality control procedures were developed to eliminate data with unphysical antenna temperatures (Ta), and other issues such as erroneous time tags, where the time of a scan could not be correctly identified. Additional quality control was required for F08, although the total amount of data flagged was less than 1%. As part of the current project, a well-documented software package was produced to create intercalibrated, quality-controlled Tb from the Ta. The software package is open-source and will be made available to the community, allowing users to create custom SSM/I Tb with their own set of corrections or apply different/updated corrections as the need arises. This software package includes modular routines that flag quality control issues, recalculate geolocation, and apply a scan nonuniformity correction, intercalibration corrections and convert from Ta to Tb using the original SSM/I antenna pattern correction [6]. Improved pixel geolocation and EIA values were calculated using updated spacecraft ephemeris from two-line element data and adjustments to the spacecraft attitude [3].

The lack of EIA information in the SSM/I TDR files has led many users to rely on the nominal values computed by Colton and Poe [6]. As shown by Berg *et al.* [3], this is inadequate for climate analyses as small changes in EIA will significantly impact the Tb's and must therefore be accounted for in both

the intercalibration and subsequent geophysical retrievals. The differences of up to 0.5° in mean EIA between sensors shown in Fig. 1(a) can lead to Tb differences of up to 1 K in the v-pol channels that will impact the subsequent intercalibration. The geolocation analysis done by Berg *et al.* [3] as part of this FCDR project estimated residual errors in the calculated EIA values of less than 0.1°, which approximately corresponds to no more than a ∼0.2-K calibration error for the 19-V channel and less for other channels.

III. Intercalibration Techniques

Five broadly different intercalibration techniques were applied to the SSM/I data. Three of these five techniques had several different implementations to give a total of ten sets of numbers, not all of which are completely independent. Through comparison of multiple intercalibration methods, we are able to better understand the inherent errors of each of the techniques and cover a wide spectrum of observed Tb's, rather than simply focusing on the colder non-cloudy/non-rainy Tb's. At the most basic level, the use of multiple approaches gives far higher confidence than the use of a single technique since independent agreement of the intercalibration estimates implies some accuracy. More importantly, the application of independent techniques gives a measure of the technique-dependent error. Our approach also utilizes several different implementations of the techniques, which gives additional insight into how sensitive these techniques are to some of the assumptions made.

Each of the techniques described below employs the same basic methodology, although the assumptions and screening applied differ. Only one of the techniques employs direct comparisons between two sensors (polar matchups). The other techniques use a transfer standard that takes the form of either matchups with another satellite (Tropical Rainfall Measuring Mission (TRMM) Microwave Imager (TMI) matchups), a numerical weather prediction model (reanalysis transfer), a fixed earth point (Amazon warm calibration), or a theoretical value (vicarious cold calibration). In all cases, it is critical to account for differences in the EIA in order to obtain a physically consistent intercalibration. This is done using several methods, but each of these involves simulating Tb's using the computed EIA for each sensor/pixel. The resulting simulated differences comprise the expected or physical component of the observed Tb difference resulting from differences in the viewing geometry between sensors. As such, they are subsequently subtracted from the total observed differences to obtain the residual difference in the sensor calibration. Each of the techniques also applies screening to ensure that only valid data (valid under the assumptions for each technique) are used. Finally, since this intercalibration is to be used for a climate record, each of the techniques was applied over the longest possible period to maximize sampling and to facilitate studies into how the intercalibration changes over time, if at all.

A. Reanalysis Transfer

One of the drawbacks for techniques involving direct comparisons (i.e., polar crossovers) is that they do not provide estimates for all SSM/I satellites. In particular, the F08 data in the FCDR has no overlaps with other satellites and so direct matchups or matchups with another reference satellite are not possible. One of the ways to address this issue is to use a radiative transfer model to simulate Tb using reanalysis data from a global forecast model. The difference between the simulated and observed Tb can then be used to calculate a residual difference for each sensor. The difference between these sensor residuals is then used to estimate the calibration difference between sensors, with the reanalysis model essentially becoming the transfer standard.

There are several potential issues with this technique that require special care. One of the biggest issues is the propagation of model errors into the calibration after taking the difference between the residuals. The first way this can occur is if different periods are used to calculate the residuals, so that either time-dependent errors or errors related to weather variations are aliased into the results. In most cases, this is addressed by using a common observing period for the two satellites, but that is not possible for F08. For F08, these issues can be greatly ameliorated by comparing F08 values with those from the first ∼2 years of F10. This should minimize the effect of potential climate trends in reanalysis model data and provide enough sampling to remove weather effects. The second potential way that model errors can affect the intercalibration comes from comparing satellites observing at different times of day. If the model has errors associated with the diurnal cycle, these can propagate into the intercalibration and might be particularly large for a model with a six-hourly time step. This issue will be excplicitly dealt with by several of the techniques. Finally, there is a potential conflict in using the reanalysis data in that most models assimilate the SSM/I data. It could be argued that the models are therefore drawn toward the original (and presumably sub-optimal) calibration of the satellite. However, the assimilation of satellite data into the reanalysis system involves bias adjustment of the satellite data to be consistent with the model, which is in itself a recalibration to the underpinning *in situ* observations. Thus, the reanalysis models use the variability of the satellites but are not biased by them, and so this problem is expected to be negligible.

In order to obtain coverage of the whole SSM/I record, reanalysis data from the National Aeronautics and Space Administration (NASA) Modern Era Reanalysis (MERRA) [12] and from the European Center for Medium Range Weather Forecasting Interim Reanalysis (ERA-I) [13] were obtained. Data were averaged to a common one-degree spatial resolution with 25 vertical layers every 3 h for MERRA and 29 vertical layers every 6 h for ERA-I. The variables used in the radiative transfer model to construct the atmospheric profile included pressure, geopotential, temperature, humidity, and liquid water as well as surface wind speed, skin temperature and surface pressure and the EIA for the corresponding satellite data. The radiative transfer model is the same as that used by Elsaesser and Kummerow [14]. Tb were gridded to one-degree resolution, and grid boxes containing the edge of scan were discarded so as to use only "full" grid boxes. An aggressive land mask was used to screen out land, and near coast gridboxes and boxes outside 60° N/S were discarded to eliminate sea ice. In addition, the standard

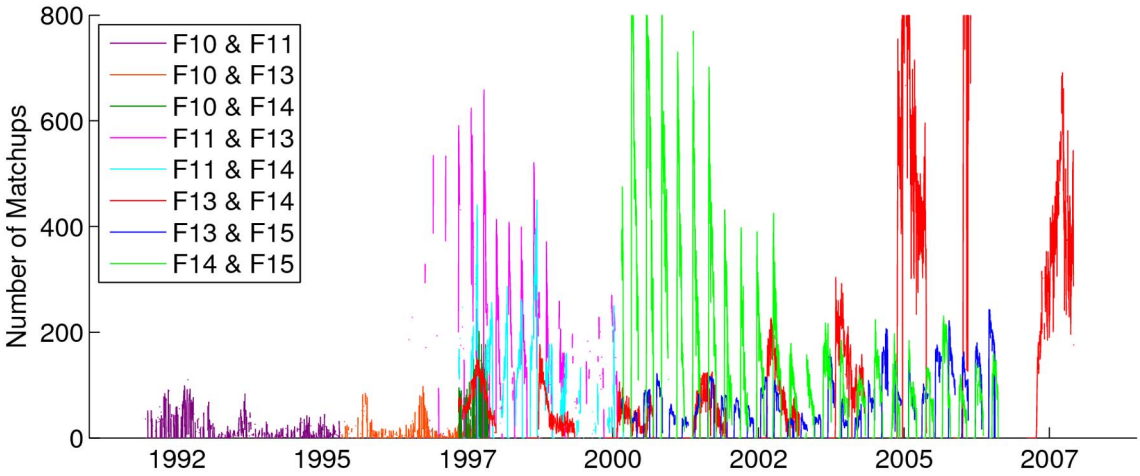

Fig. 2. Time series of number of direct polar matchups between each of the SSM/I satellites.

deviation of the 85 GHz Tb in the one-degree box was used to screen out clouds and rain by eliminating those with a value greater than 3 K. This threshold was chosen by trial-and-error to minimize contaminated pixels, while retaining enough sampling. It was also found to be necessary to screen for clouds and rain in the model profiles, so these were removed when total column liquid water exceeded 0.01 kg m^{-2}. The model grid box closest in time to the observations was then selected and used to compute simulated Tb for comparison with observed Tb.

B. Polar Crossover

The SSM/I instruments were flown with the goal of having dual coverage with one sensor crossing the equator at around 6 A.M./P.M. (descending/ascending) and another around 8 A.M./P.M. [Fig. 1(a)]. Since they were flown on the sun-synchronous polar orbiting DMSP, the only direct overlaps between SSM/I sensors occur near the poles. Direct polar matchups were not possible for F8 since that sensor did not significantly overlap in time with any of the others (see Table I).

Coincident observations or crossovers between sensors were defined as those occurring within 30 min of each other. Two methods were tested for obtaining matched data. The first method involved matching individual pixels within 50 km and 30 min. The second method involved gridding the data onto a roughly 100 km equal-area global grid and then matching grid boxes. Similar results were found for each of the methods, but the second method provides a number of advantages. First, in order to account for differences in EIA between the two sensors, it was necessary to match one-degree reanalysis model data to the crossovers and the gridded data are more comparable to the reanalysis data than the pixel data. Second, the gridded data made it easier to screen out clouds by using the standard deviation of the 85-GHz Tb within the grid box. Fig. 2 shows a time series of the number of matchups between each pair of sensors using the one-degree averaged technique. The number of matchups differs according to the season and the equator crossing times (which are subject to orbit drift) of the satellites being matched. While not all matchups had sufficient crossovers for comparison, satellites with similar crossing times had more matchups.

Once the matchups were identified, a liberal land mask was used to screen out grid boxes over land as well as near the coast. Ice concentration from the "National Ice Center Arctic sea ice charts and climatologies in gridded format" data set [15] was used to identify grid boxes that were completely ice free (open ocean). Cloud-free grid boxes were identified using the standard deviation of the 85 v and 85 h channels within each grid box, with only those boxes with a value less than 3 K being used. Profile data from MERRA were gridded to the same equal area grid and used to simulate Tb for each sensor based on the EIA. The difference between the simulated Tb for the two sensors was then subtracted from the difference between the observed Tb to obtain the intercalibration difference between those two sensors.

C. TMI Matchups

TMI has a very similar channel complement to SSM/I and due to its low inclination orbit, which samples the full diurnal cycle, it can be used as a transfer standard to eliminate the impact of diurnal cycle variability while providing direct matchups at low latitudes. While TMI is very similar in design to the SSM/I (TMI was based on the SSM/I design), it has a different view angle to SSM/I as well as some slight differences in channel frequencies, particularly the water vapor channel, which is at 21.3 GHz for TMI. Another drawback of this approach is that TRMM was launched in late 1997 meaning that data are not available for intercalibrating F08 and F10, and there are only $\sim$2 years of overlap for F11.

As with the polar crossovers technique, ground-tracks for each satellite were used to identify crossovers between each of the SSM/I sensors and TMI. Tb were averaged onto a one-degree latitude/longitude grid, with grid-boxes containing the edge-of-scan discarded to obtain only "full" boxes. A land mask was used to remove land pixels (sea ice was not a problem since TRMM flies at an inclination of 35°) and the standard deviation of the 85 GHz Tb was used to remove rain/cloud scenes. For the SSM/I and TMI comparisons, not only do differences in EIA

need to be accounted for, but also the differences in channel frequencies.

In order to better understand potential errors in the simulated Tb associated with channel and EIA differences, three different techniques were used to estimate these differences. Note that all three of these approaches use the same radiative transfer model. The first technique involved the retrieval of geophysical parameters from TMI using the optimal estimation (OE) technique described in Elsaesser and Kummerow [14]. This OE technique is an iterative approach to inverting a radiative transfer model to obtain estimates of wind speed, total precipitable water (TPW) and cloud liquid water that are consistent with the observed Tb and the specified sea surface temperature ([16]). The retrieved geophysical variables were then used to simulate Tb for both TMI and SSM/I to account for differences in EIA and channel characteristics including frequency. The other two techniques used to account for EIA and channel differences are similar to the technique described for the reanalysis transfer intercalibration technique. The reanalysis surface and profile data from MERRA and ERA-I were used to simulate the expected Tb differences between TMI and SSM/I, providing two additional realizations of these differences based on reanalysis data.

D. Vicarious Cold Calibration

As previously mentioned, one of the challenges in intercalibrating the SSM/I record is connecting F08 to F10 and hence the rest of the series. Since there are no direct overlaps with any other radiometer, some other transfer standard must be used for F08. Tb simulated from reanalysis data have already been mentioned as a method that can be used for this purpose, but another approach is to use the vicarious calibration method described by Ruf [17]. The approach exploits the property that the minimum Tb over the open ocean occurs at a fixed sea-surface temperature that varies by channel and EIA. The technique involves estimating the minimum Tb over the open ocean using a statistical approach. There are still several drawbacks to this approach, most importantly that the theoretical minimum Tb for the 85-GHz channels occurs at a Tb that is not regularly observed over the open ocean. The technique instead provides an estimate of the observed statistical minimum for the 85-GHz channels.

Histograms of Tb for each channel were calculated from the overlap period for the two sensors to be compared. The Tb were screened to remove scenes with high values of atmospheric water vapor so that the histograms represent only the cold end of oceanic Tb. A polynomial fit was then used to estimate the minimum Tb from the histogram. The EIA dependence was removed by repeating the procedure using simulated Tb based on the OE, Merra, and ERA-I profiles. The minimum can be distorted by changes in the water vapor distribution over time, so a common period of overlap was used to estimate the vicarious cold minimum. In the case of F08, there is no overlap with the other sensors and so two years of F08 data were compared to four different years of F10 data. While not overlapping, the use of relatively short periods that are close in time should ameliorate the effect of any water vapor changes that would be expected to occur on longer timescales.

E. Amazon Warm Calibration

The techniques presented so far are limited to open-ocean, cloud/free Tb, which correspond to the colder part of the spectrum of observed Tb. It is desirable to have an estimate of the differences between the satellites over the warm part of the spectrum in order to determine if there is any slope (gain) in the intercalibration differences. The warmer Tb are predominantly observed over land due to the much higher surface emissivities. This complicates the radiative transfer modeling and can lead to larger errors and the techniques described so far are not sufficient for this purpose. For an estimate of the intercalibration at the warm end, we used the technique described by Brown and Ruf [18], which is based on identifying a relatively large, near-blackbody target on earth and using crossovers from each of the satellites to estimate intercalibration values. The target and methodology used in this study is the same as that used by Brown and Ruf [18], who used a homogeneous area over the Amazon as the target. Once crossovers over the target area were obtained, a physical model described by Brown and Ruf [18] was used to simulate Tb for each sensor so that the target area could be used as a transfer standard. The error of the physical model was estimated by Brown and Ruf [18] as 0.57 K.

One of the major issues with the application of this technique to the SSM/I record is the effect of the diurnal cycle, which is relatively large over land. As shown in Fig. 1(a), the SSM/I sensors rarely observed the same time of day. In addition, satellite orbit drift leads to changes in the observing time that could result in trends in the intercalibration that are aliased with the diurnal sampling. In order to remove any diurnal effect, the comparisons were done using TMI as a transfer standard since its orbit provides samples throughout the day. Matchups with SSM/I and TMI over the target area were used to estimate the intercalibration for the SSM/I relative to the TMI. These matchups were therefore obtained only for F13, F14, and F15 since they have long overlaps with TMI. The SSM/I-TMI comparisons were then used to estimate the intercalibration values between each combination of F13, F14, and F15. The original technique was extended for use with the SSM/I high-frequency channels by extrapolating the linear dependence of the single scatter albedo on frequency used in the original Brown and Ruf [18] formulation to 85 GHz. This extrapolation is justified by the emissivity retrievals of Prigent *et al.* [19] using SSM/I data over dense vegetation. As was done by Brown and Ruf [18], only 85-GHz data for which the v, h difference was less than 3 K were used to select de-polarized, near-blackbody regions. To ensure the quality of the resulting Amazon reference parameters, only retrievals for which the root mean squared fitting error was less than 1.5 K were used. At this threshold, 95% of the data that met the 3 K v/h difference requirement remain.

IV. Results

The five techniques described in Section III were applied to the SSM/I FCDR record with all of the quality control and

TABLE II
SUMMARY OF TECHNIQUES USED TO ESTIMATE INTERCALIBRATION

Technique	Simulation of Tb	Simulation resolution	Sensors covered	Notes
Polar Matchups	ERA-I	1° equal area grid	F10, F11, F13, F14, F15	Matchups within 30 mins; Cloud screen: 85GHz<3 K
Reanalysis Transfer	Merra, ERA-I	1° grid	F08, F10, F11, F13, F14, F15	Limited to 60°N/S; Cloud screen: 85GHz<3 K & Model Liqud Water < 10g/kg
TMI Matchups	Merra, ERA-I, Optimal Estimation	1° grid	F11, F13, F14, F15	Matchups within 30 mins; Cloud screen: 85GHz<3 K
Vicarious Cold	Merra, ERA-I, Optimal Estimation	Native resolution	F08, F10, F11, F13, F14, F15	Cloud screen: 85GHz<3 K
Amazon Warm	Physical model developed in [18]	Native resolution	F13, F14, F15	TMI used as transfer standard

other corrections applied (see Section II), but no intercalibration correction. As described, multiple methods to simulate the expected Tb differences were used to assess uncertainties in the techniques, which are summarized in Table II. The reanalysis transfer technique was implemented using both Merra and ERA-I reanalysis. The Tb simulations for the TMI matchup and the vicarious cold calibration techniques were implemented using geophysical retrievals from the OE, Merra, and ERA-I. The direct polar matchups and Amazon warm calibration techniques do not have multiple realizations. Thus, there are up to ten different sets of numbers that must be combined to provide the final intercalibration estimate, although as previously described not all of the techniques can be applied for all of the sensor combinations, particularly early in the record. In this section, the implementations are compared to assess differences and sources of errors and then the ten techniques are compared to assess overall agreement. A strategy for combining these ten techniques is presented and rudimentary error estimates based on the spread of the techniques are calculated.

A. *Comparison of Techniques*

The use of multiple techniques gives confidence in the results, assuming they all agree within some tolerance, but also allows for a different kind of characterization of the error of the combined estimate by considering the spread among the techniques. Fig. 3 shows the intercalibration estimates between F13 and F15 for each channel from each of the techniques listed in Table II as a function of the F13 Tb. We start with F13 minus F15 because these two sensors had a significant overlap with results from all techniques and these sensors as well as quite different diurnal sampling as shown in Fig. 1. The first thing to note is that the agreement between the techniques is good for all channels with peak-to-peak differences typically within 0.5 K. This high level of agreement between techniques was found for all sensor combinations with sufficient sampling and provides a high level of confidence in the results from each technique. As already stated, most of the techniques use observations at the colder end of the Tb spectrum. The Amazon warm calibration technique is the only technique in this study that provides an estimate at the warm end and the agreement with the other techniques tends to be poorer with differences up to ∼1 K.

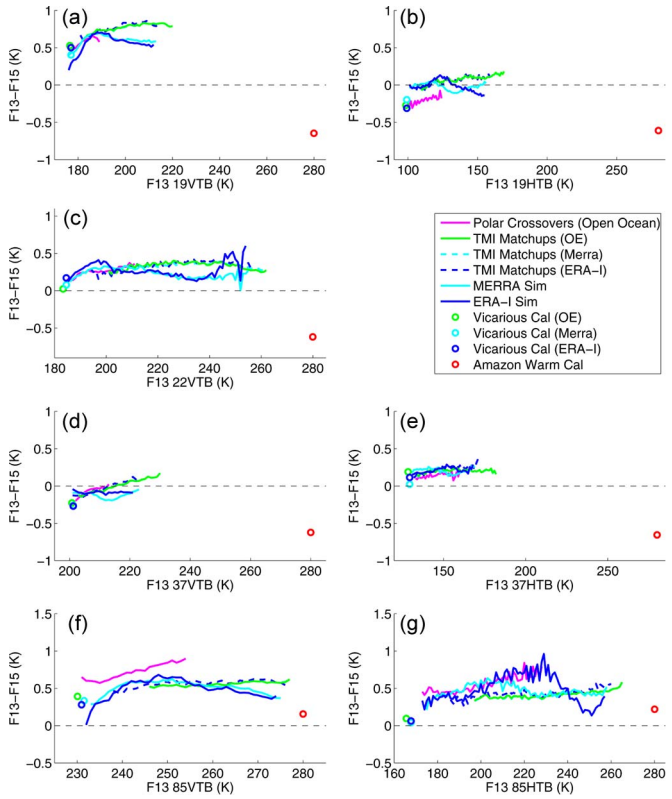

Fig. 3. Intercalibration estimates for SSM/I F13 minus F15 as a function of F13 Tb for each of the seven channels. Lines represent Tb bins where the sampling was sufficient to produce an estimate.

A critical issue for the intercalibration is whether the techniques cover the entire range of observed Tb. Fig. 4 shows histograms of Tb by channel derived from F13 for the year 2006 by surface type (based on the flag given in the original TDR files). Not surprisingly, the range of values for each channel is consistent with the location of the results on Fig. 3 with the Amazon warm calibration around the peak of the Tb range over land, whereas the other techniques tend to cover the range of observed ocean values. One of the main issues in designing a strategy for the combination of the techniques is whether the intercalibration should depend on scene temperature. The implications of the spread of results seen on Fig. 3 for combination of these techniques are important for this question. In channels where the range of observed Tb is not well covered by the "cold" techniques (i.e., 19 V, 19 H, 37 V, 37 H), the Amazon warm calibration technique is comparatively more useful, although that technique is subject to increased error due to the additional uncertainties introduced when simulating Tb over vegetation. This issue will be revisited when describing the combination of results with error information for the Amazon warm calibration.

The results shown in Fig. 3 for F13 minus F15 were produced for all combinations of SSM/I sensors with overlap greater than three years (not shown). The agreement between techniques for each sensor combination was generally similar to that for F13 minus F15, although the number of available techniques is reduced for the earlier sensors. In particular, there were no direct overlaps for F08 so the vicarious cold and reanalysis transfer techniques must be relied upon to intercalibrate F08.

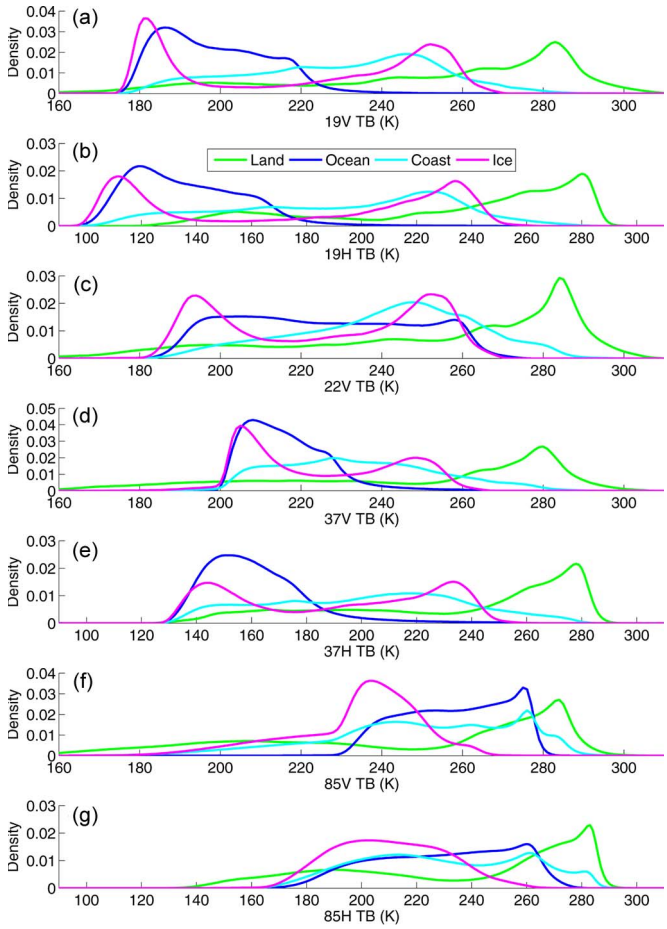

Fig. 4. Histograms of Tb values covered by each of the SSM/I channels for four surface types. The histograms were produced from one year of F13 data (2006) with the surface types taken from the flag in the original TDR files, which is preserved in the base files.

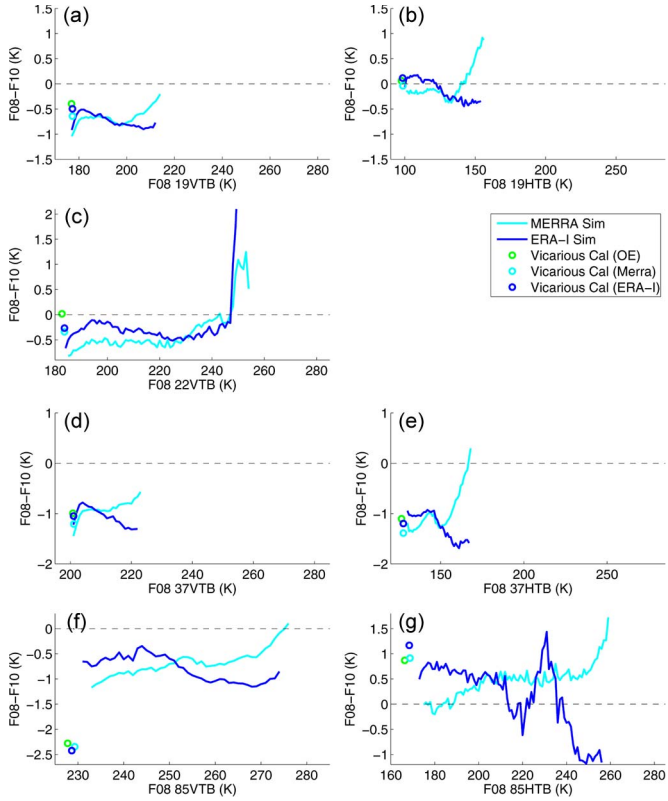

Fig. 5. As Fig. 3, but for SSM/I F08 minus F10.

Making matters worse, the 85 V channel on F08 failed around January 1989 meaning that the full F08 record is essentially restricted to July 1987–December 1988 For the comparison of F08 minus F10, this period was compared with F10 results from December 1990 through December 1994. The comparison of F08 minus F10 is shown in Fig. 5 (note that the color scheme is different from Fig. 3). The agreement between the techniques is still generally good, although there is more noise in the reanalysis model simulations. The agreement between the Tb is around $\sim$1 K for most channels apart from the 85 V, where there is a $\sim$1.5-K difference between the vicarious cold techniques and the reanalysis transfer techniques. The range of values covered by these techniques is far more limited than that for Fig. 3. Given this and the reduced set of techniques, it is expected that the earlier satellites should have a higher error attached to their intercalibration.

B. Differences Between Implementations

Given that all of the intercalibration techniques described above rely on radiative transfer simulations to account for differences in EIA between sensors, one of the main concerns is that deficiencies in the simulation procedure might propagate into the results. The sometimes-large differences between the observed and simulated Tb can be ameliorated with careful screening of pixels that are inconsistent with assumptions of the radiative transfer model, such as the presence of rain or sea ice. The residual differences tend to largely cancel out when the double difference between sensors is calculated. With that in mind, a further distinction should be drawn between the reanalysis transfer and TMI matchup techniques. The main advantage of the TMI matchup technique is that the SSM/I and TMI observations are coincident in time so as to remove the effect of the diurnal cycle. The reanalysis transfer technique does not have this characteristic and instead relies on the reanalysis model to correctly represent the diurnal cycle. Errors that do exist in the diurnal cycle have the potential to propagate into the intercalibration estimate for combinations of satellites that make observations at significantly different local times [see Fig. 1(a)]. In reality, the reanalysis models are known to poorly represent the diurnal cycle, although errors due to the diurnal cycle are likely to be smaller over the ocean where the calibration numbers are obtained. Nevertheless, great care must be taken when comparing satellites using the reanalysis transfer approach.

One of the major uncertainties in the reanalysis transfer approach is the temporal resolution of the reanalysis data. Data were available at three-hour resolution for Merra and at six-hour resolution for ERA-I, with observations being instantaneous rather than time averaged. The Tb were simulated using the reanalysis profile nearest in time to the observation. Thus, the time difference between the simulations and observations can be up to 1.5 h for Merra and up to three hours for ERA-I. It may, therefore, be reasonable to expect that the estimates from ERA-I might be more affected by errors in the diurnal cycle

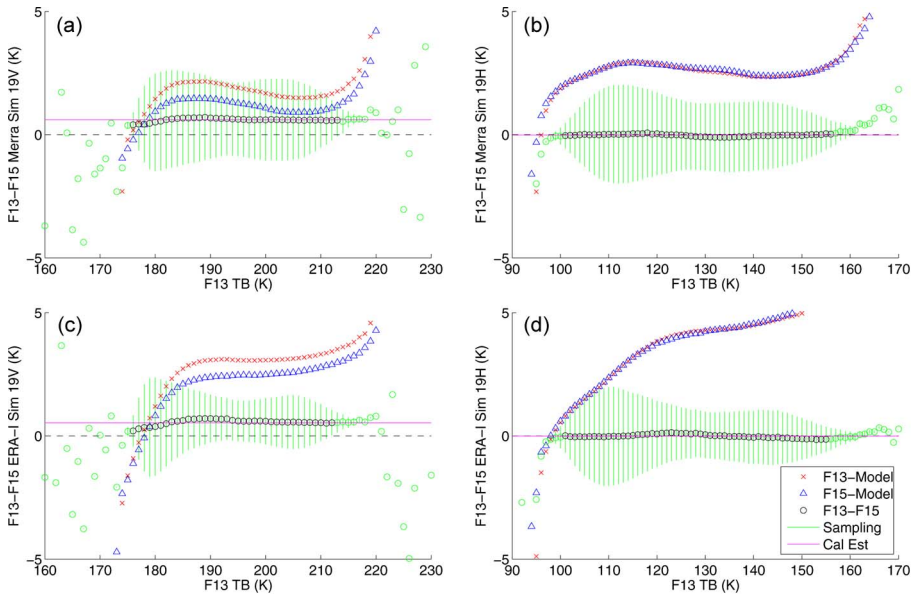

Fig. 6. Comparison of reanalysis model simulation results for SSM/I F13 versus F15 for the 19 V and 19 H channels. The green lines that denote sampling are simply the total number of samples normalized for plotting. The black circles denote difference values used in the estimation of the calibration estimate (magenta line).

than those from Merra, assuming the reanalysis models have similar diurnal cycle errors. Fig. 6 shows the mean observed minus simulated 19 GHz Tb as a function of scene temperature from F13 and F15 for both Merra and ERA-I. The black circles show the intercalibration estimate derived from the difference between the observed minus simulated for F13 and F15. The intercalibration estimate is only evaluated when there is sufficient sampling as denoted by the green lines. Both channels and both reanalyzes show clear disagreement between the observed and simulated Tb with errors of 1–5 K. Errors in simulated Tb vary as a function of scene temperature in all cases, although there appears to be a strong sampling dependence. The scene temperature dependence is largest for the 19-h simulations using ERA-I as shown in Fig. 6(d), which far exceeds the temperature dependence of simulated Tb errors based on Merra. This scene-dependent error in the 19 H for ERA-I does not, however, lead to a scene temperature dependence, as indicated by the magenta line. Coupled with the fact that the simulated Tb from Merra do not have the scene temperature dependence, this suggests that the errors are an artifact of the different mode reanalysis time steps. As mentioned previously, however, by double differencing the observed and simulated Tb between sensors, the resulting intercalibration values are relatively insensitive to the large simulation errors. A somewhat similar conclusion can be drawn from the 19 V, where some scene dependence is observed around 180 K in simulation from both reanalyses. This 0.5-K drop in the intercalibration follows the same pattern as the observed minus simulated lines for F13 and F15 and appears to be an artifact of the technique, although it has no discernable effect on the overall mean as shown by the magenta line.

As mentioned previously, the TMI matchup technique has the advantage over the reanalysis transfer technique in that the use of TMI as a transfer standard eliminates any diurnal cycle dependence. This is a significant advantage given the changing observing times of the satellites. Differences between the TMI and SSM/I view angles and water vapor channels (the water vapor channel for TMI is at 21.3) may have a larger impact on the simulated Tb, although once again this effect is largely removed by double differencing.

Fig. 7 shows the residual calibration difference between F13 and TMI after removing the simulated channel and EIA differences using simulations from Merra, ERA-I and the OE. The values represented on Fig. 7 should be interpreted in a similar way to the black circles on Fig. 6 in that they are corrected comparisons between two sensors. There are signs of small scene-dependent variations in the calibration in several of the channels, most notably the 19 H, 22 V, 85 v and 85 H, although the other channels are not completely flat. Interestingly, the 19 V shows a similar (but inverted) behavior to that for F13 minus F15 shown in Fig. 6(a), which is probably caused by reanalysis model error that is small and will be averaged out of the final intercalibration numbers.

Comparison of the three techniques reveals that the simulated Tb based on the OE and the two reanalyses are usually in excellent agreement with differences typically around $\sim$0.1 K in most channels. The exception to this is the 22-V water vapor channel, where the disagreement is slightly larger between the OE and the reanalyses probably reflecting differences, and perhaps deficiencies, in the representation of water vapor. In the case of the 22 V, the disagreement is $\sim$1 K but is reduced at higher scene temperatures. In practice, these differences between implementations will largely cancel out for the SSM/I comparison, but this is another source of uncertainty for the techniques.

C. Combination Of Intercalibration Estimates

A number of issues have already been presented that must be considered when combining results from the intercalibration techniques. Although there are some differences between

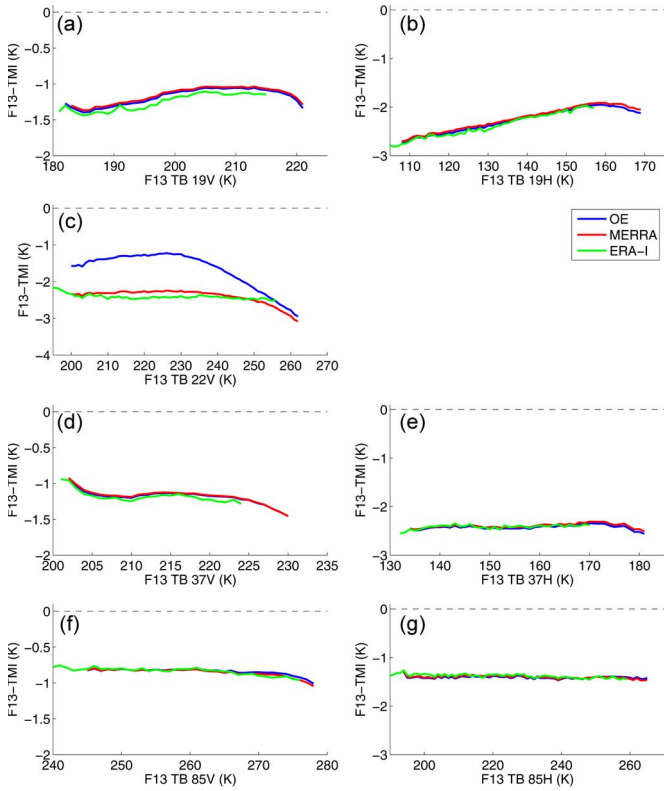

Fig. 7. Plots comparing the agreement between TMI and SSM/I F13 for each channel using the three simulation techniques (optimal estimation, simulations from Merra and ERA-I).

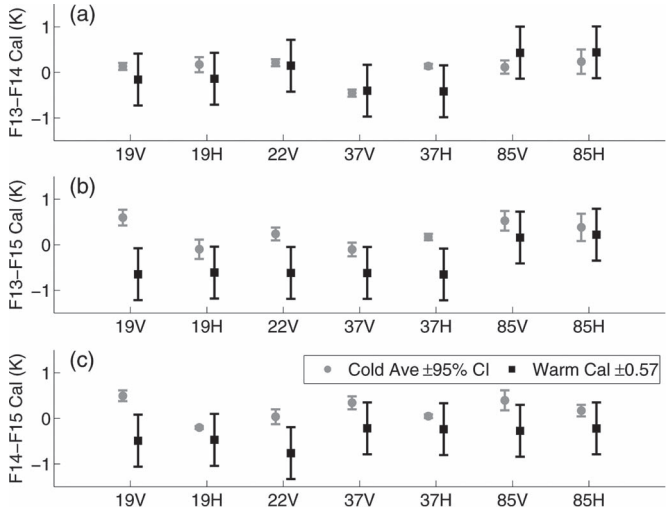

Fig. 8. Comparison of Amazon warm calibration estimate with the average of the other techniques, which are all at the cold end of the Tb range. Error bars for the Amazon warm calibration estimate are based on the published value of 0.57 K [18]. Error bars for the average of the cold techniques denote the 95% confidence interval for the mean based on the t-distribution with three degrees of freedom.

various implementations of the techniques, these are small compared to the spread among techniques. A simple average of all ten implementations, as shown for F13 versus F15 in Fig. 3, would skew the result toward the TMI matchup and vicarious cold calibration techniques that have three implementations each. The first step in the combination procedure is therefore to average the results from the different implementations to obtain a single set of values as a function of Tb from each of the five techniques. Differences between these implementations will not be used in the overall error estimate, but it should be noted that the averaging improves the precision of each technique.

One of the most critical decisions for the combination of results is whether a temperature-dependent correction should be applied. We have adopted a "first do no harm" approach to correcting the FCDR and as such a simple offset is preferred unless it is apparent that a scene temperature-dependent component is required. The use of a slope in the intercalibration can be problematic in the case where extrapolation beyond the range of Tb used in the intercalibration can lead to unrealistic values that can be deleterious for geophysical retrievals. For example, if one were to apply a slope to the intercalibration between F08 and F10 based on the results in Fig. 5, it could result in unrealistic and thus poorly calibrated values over land and other warm scenes. Fig. 8 shows a comparison of the Amazon warm calibration with the average of the nine "cold" techniques. The error bars for the Amazon warm calibration are 0.57 K as suggested by Brown and Ruf [18], whereas the error bars on the average of the four cold end techniques are 3.18 multiplied by the standard error of the mean, which gives a 95% confidence interval for the mean based on the t-distribution with three degrees of freedom. In reality, the standard error of the mean of the techniques is a less reliable measure if there is an absolute bias in the mean of the techniques, but it provides a useful indication of the spread. In nearly all cases, the difference between the mean of the four techniques and the Amazon warm calibration is less than the 0.57 K error of the latter technique, which suggests that a scene temperature-dependent correction is not warranted. At this point, there is insufficient information to suggest a temperature-dependent intercalibration between the SSM/I sensors, which is perhaps unsurprising given the similarity of the sensors. The consequence of using an offset is that we have a relatively high amount of confidence with this calibration for retrievals like TPW that occur over cold scenes, but much less for intense precipitation where the Tb may be substantially warmer.

The mean for each combination of satellites was obtained by finding the mean of the estimates from the five techniques. The standard error of the mean was then derived for each combination as the standard deviation divided by the square root of the number of techniques. F13 was chosen as the calibration standard because it provides the longest record, has direct overlaps with three of the other sensors, and had a stable equator crossing time (see Fig. 1). Direct overlaps with F13 were not possible for F08, so a more circuitous approach was required where F08 was intercalibrated to F13 via F10. The standard errors for F08 were obtained using the same overlaps.

The final combined intercalibration offsets for each of the SSM/I sensors are shown in Table III. The values for F14 and F15 compared to F13 are relatively small, which reflects the fact that these sensors were fabricated at the same time and had similar, high-quality control standards. The earlier sensors tend to require larger intercalibration offsets that perhaps reflect modifications in the latter sensors through the ongoing SSM/I calibration/validation process. F08 in particular requires offsets

TABLE III
MEAN CALIBRATION FOR EACH OF THE SSM/I COMPARED TO F13. VALUES FOR F14 AND F15 THAT EXCLUDE THE AMAZON WARM CALIBRATION TECHNIQUE ARE ALSO INCLUDED. THE STANDARD ERROR OF THE ESTIMATES IS INCLUDED IN BRACKETS. ALL QUANTITIES ARE IN KELVINS

Mean (SE)	19V	19H	22V	37V	37H	85V	85H
F08	0.65 (0.05)	0.16 (0.04)	1.42 (0.07)	0.82 (0.03)	1.64 (0.05)	1.91 (0.41)	-0.52 (0.20)
F10	0.05 (0.03)	0.16 (0.04)	1.27 (0.09)	-0.21 (0.01)	0.48 (0.04)	0.37 (0.07)	0.11 (0.13)
F11	0.19 (0.01)	-0.16 (0.03)	0.15 (0.05)	0.67 (0.02)	0.36 (0.02)	-0.55 (0.05)	-1.22 (0.11)
F13	0.00 (0.00)	0.00 (0.00)	0.00 (0.00)	0.00 (0.00)	0.00 (0.00)	0.00 (0.00)	0.00 (0.00)
F14	0.34 (0.11)	-0.20 (0.05)	0.06 (0.08)	-0.20 (0.05)	0.00 (0.07)	0.45 (0.04)	0.35 (0.04)
F15	0.29 (0.09)	-0.26 (0.02)	-0.13 (0.07)	0.24 (0.05)	-0.00 (0.03)	0.26 (0.07)	0.09 (0.04)
F14 (Cold Cal)	0.59 (0.03)	-0.10 (0.04)	0.23 (0.02)	-0.10 (0.03)	0.17 (0.01)	0.53 (0.04)	0.38 (0.05)
F15 (Cold Cal)	0.49 (0.02)	-0.21 (0.00)	0.03 (0.03)	0.35 (0.03)	0.05 (0.01)	0.39 (0.04)	0.17 (0.02)

larger than 1 K for three of the channels, but even these offsets are relatively small due to the common design of the sensors. For F14 and F15, the mean intercalibration includes the Amazon warm calibration values which lead to higher standard errors than when they are excluded (denoted as "cold cal" estimates in Table III). The inclusion of the Amazon warm calibration estimates changes the calibration by as much as 0.2 K in some cases, which is a relatively small offset for most purposes. For the purposes of estimating the error of the final estimates, it is important to note that these estimates from the five techniques are not completely independent. For example, they share a common radiative transfer model, which mean that the standard error does not represent the full range of possible errors from these sources.

D. *Effect of Intercalibration Offsets on Retrieved Parameters*

The offsets developed in this work will be applied to the SSM/I FCDR that will be used for retrieving geophysical parameters suitable for climate studies. Although the nature of the values in Table III is preliminary, the FCDR has been used to produce long precipitation and water vapor time series (see [3, Fig. 12]), and the results of these tests show an improvement in the consistency of the long-term water vapor data record. The OE retrieval was therefore used to investigate the impact of the calibration on estimates of TPW. Because the magnitude of the diurnal cycle of TPW is large relative to the changes in TPW associated with the intercalibration and differences caused by the diurnal cycle are not corrected in the FCDR, a direct comparison between retrievals from two SSM/I cannot be used to evaluate the impact of the calibration. Fig. 9, however, shows maps of differences between the retrieved TPW based on both the original and intercalibrated Tb for each sensor. Differences were calculated on a single January for each sensor. A map of the mean TPW from F13 for January 1996 is also included for reference since no intercalibration is applied to F13. The differences tend to mirror the mean observed patterns with larger differences occurring in areas of higher TPW. This is reversed for F10, likely due to relative differences in the calibration between channels. The largest differences occur for

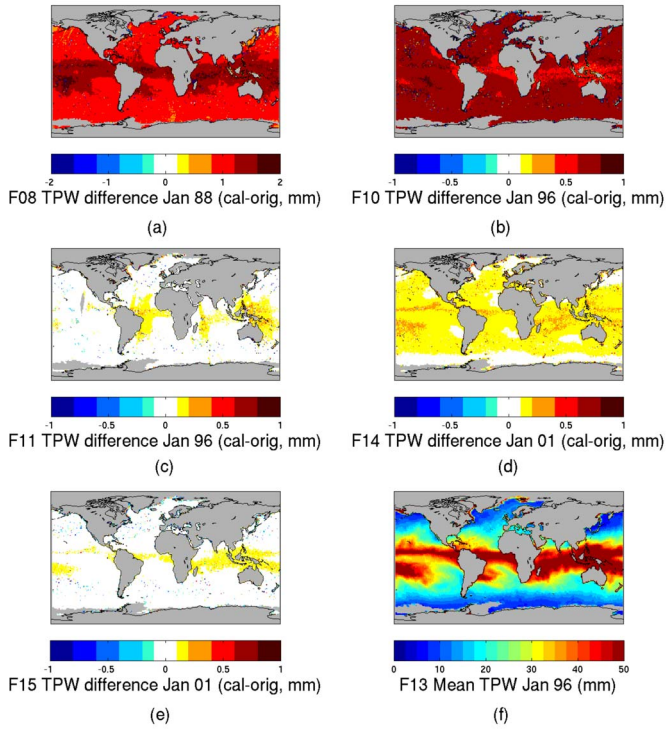

Fig. 9. Differences between retrieved TPW based on the intercalibrated Tb minus TPW estimates based on original Tb in mm. Plots are based on a single month: January 1988 for F08, January 1996 for F10 and F11, January 2001 for F14 and F15. (f) shows the mean TPW field from F13 for January 1996, also in mm.

F08 and F10, which had larger intercalibration offsets applied (Table III). Differences are around 1–1.5 mm for F08 which is $\sim$2% of the mean and is definitely not negligible for climate applications (the Intergovernmental Panel on Climate Change gave the trend in SSM/I monthly water vapor as 1.2% per decade [20]). The difference is somewhat smaller for F10, $\sim$0.7 mm, but such differences tend to be larger outside the tropics where mean TPW is lower, and so these differences are amplified (5%–10%). Differences are far smaller for F11, F14, and F15, and reflect the smaller intercalibration offsets for these sensors. These differences are $\sim$0.5%, but can still be important for sensitive climate studies. While it is challenging to quantify agreement between the intercalibrated sensors and F13 due to real, physical differences associated with diurnal and other variability, Fig. 9 shows that the intercalibration offsets derived here are of a sufficient magnitude to be important for climate studies.

V. SUMMARY

Five independent techniques have been presented for the intercalibration of the complete SSM/I record (excluding the F15 RADCAL affected period) from 1987 to 2009. The SSM/I data have been quality-controlled and new geolocation has been calculated using previously derived estimates of satellite attitude to obtain accurate EIA estimates for each satellite. Multiple realizations of each of the five techniques were used to simulate expected Tb differences resulting from differences in EIA, including the use of two different reanalysis data sets as

well as an OE-based retrieval technique. Most of the techniques give estimates toward the cold end of the range of observed Tb, with the exception of the Amazon warm calibration that can be used to determine whether a scene temperature-dependent correction is required.

Excellent agreement was found between the various techniques, with a spread of $\sim$0.5 K for the more recent sensors and a spread of $\sim$1 K for F08 and F10. The level of agreement between these results gives a high level of confidence in the techniques, but obtaining such good agreement required careful implementation of the techniques. Perhaps the most important consideration was the use of consistent input data and screening techniques in order to remove pixels that were inconsistent with the assumptions of the radiative transfer model. Additionally, the use of accurate pixel-based estimates of EIA instead of using nominal EIA values was a major factor in ensuring that erroneous differences were ameliorated.

A method for combining the estimates to obtain a single calibration offset was presented and applied. In the case of F13, F14, and F15, warm end intercalibration numbers were obtained and used in the estimate. The difference between the warm and cold intercalibrations was generally less than the error in the warm end estimate, and so an offset was deemed appropriate, although this may need to be re-evaluated if information comes to light that suggests a temperature-dependent slope in the intercalibration between sensors.

Not all of the techniques were applicable over the entire data record so care is required in assembling intercalibration offsets for the whole period of record. In addition, the errors are expected to be larger toward the start of the record when the range of applicable techniques is more limited. This meant that some modifications to the approach used to combine the results were required in order to transfer the intercalibration back to F08 from F13, which involved using a combination of overlapping sensors. The actual intercalibration values tended to be small for the more modern sensors (F11, F13, F14, F15) but intercalibration offsets were up to 2 K for the older sensors (F08, F10). Errors were correspondingly larger for the earlier satellites, reflecting less good agreement between the few available techniques. In addition, errors were larger when the warm end results were included, which reflects the higher uncertainty in that technique.

ACKNOWLEDGMENT

The authors are grateful for the input of the members of the NASA Global Precipitation Mission Working Group on Intercalibration.

REFERENCES

[1] J. P. Hollinger, J. L. Peirce, and G. A. Poe, "SSM/I instrument evaluation," *IEEE Trans. Geosci. Remote Sens.*, vol. 28, no. 5, pp. 781–790, Sep. 1990.

[2] K. A. Hilburn and F. J. Wentz, "Mitigating the impact of RADCAL beacon contamination on F15 SSM/I ocean retrievals," *Geophys. Res. Lett.*, vol. 35, no. 18, pp. L18806-1–L18806-3, Sep. 2008.

[3] W. Berg, M. R. P. Sapiano, J. Horsman, and C. Kummerow, "Improved geolocation and earth incidence angle information for a fundamental climate data record of the SSM/I sensors," *IEEE Trans. Geosci. Remote Sens.*, vol. 51, no. 3, pp. 1504–1513, Mar. 2013.

[4] F. Wentz, "A well-calibrated ocean algorithm for special sensor microwave/imager," *J. Geophys. Res.*, vol. 102, no. C4, pp. 8703–8718, Apr. 1997.

[5] S. Yang, F. Weng, B. Yan, N. Sun, and M. Goldberg, "Special Sensor Microwave Imager (SSM/I) intersensor calibration using a simultaneous conical overpass technique," *J. Appl. Meteorol. Climatol.*, vol. 50, no. 1, pp. 77–95, Apr. 2011.

[6] M. C. Colton and G. A. Poe, "Intersensor calibration of DMSP SSM/I's: F-8 to F-14, 1987–1997," *IEEE Trans. Geosci. Remote Sens.*, vol. 37, no. 1, pp. 418–439, Jan. 1999.

[7] A. Andersson, K. Fennig, C. Klepp, S. Bakan, H. Graßl, and J. Schulz, "The hamburg ocean atmosphere parameters and fluxes from satellite data—HOAPS-3," *Earth Syst. Sci. Data*, vol. 2, no. 2, pp. 215–234, Sep. 2010.

[8] A. Royer and S. Poirier, "Surface temperature spatial and temporal variations in North America from homogenized satellite SMMR-SSM/I microwave measurements and reanalysis for 1979–2008," *J. Geophys. Res.*, vol. 115, no. 8, pp. D08110-1–D08110-16, Apr. 2010.

[9] W. N. Meier, S. J. S. Khalsa, and M. H. Savoie, "Intersensor calibration between F-13 SSM/I and F-17 SSMIS near-real-time sea ice estimates," *IEEE Trans. Geosci. Remote Sens.*, vol. 49, no. 9, pp. 3343–3349, Sep. 2011.

[10] D. B. Kunkee, G. A. Poe, D. J. Boucher, S. D. Swadley, Y. Hong, J. E. Wessel, and E. A. Uliana, "Design and evaluation of the first special sensor microwave imager/sounder," *IEEE Trans. Geosci. Remote Sens.*, vol. 46, no. 4, pp. 863–883, Apr. 2008.

[11] B. Yan and F. Weng, "Intercalibration between special sensor microwave imager/sounder and special sensor microwave imager," *IEEE Trans. Geosci. Remote Sens.*, vol. 46, no. 4, pp. 984–995, Apr. 2008.

[12] M. M. Rienecker, M. J. Suarez, R. Gelaro, R. Todling, J. Bacmeister, E. Liu, M. G. Bosilovich, S. D. Schubert, L. Takacs, G.-K. Kim, S. Bloom, J. Chen, D. Collins, A. Conaty, A. da Silva, W. Gu, J. Joiner, R. D. Koster, R. Lucchesi, A. Molod, T. Owens, S. Pawson, P. Pegion, C. R. Redder, R. Reichle, F. R. Robertson, A. G. Ruddick, M. Sienkiewicz, and J. Woollen, "MERRA—NASA's modern-era retrospective analysis for research and applications," *J. Climate*, vol. 24, no. 14, pp. 3624–3648, Jul. 2011.

[13] D. P. Dee, S. M. Uppala, A. J. Simmons, P. Berrisford, P. Poli, S. Kobayashi, U. Andrae, M. A. Balmaseda, G. Balsamo, P. Bauer, P. Bechtold, A. C. M. Beljaars, L. van de Berg, J. Bidlot, N. Bormann, C. Delsol, R. Dragani, M. Fuentes, A. J. Geer, L. Haimberger, S. B. Healy, H. Hersbach, E. V. Hólm, L. Isaksen, P. Kållberg, M. Köhler, M. Matricardi, A. P. McNally, B. M. Monge-Sanz, J.-J. Morcrette, B.-K. Park, C. Peubey, P. de Rosnay, C. Tavolato, J.-N. Thépaut, and F. Vitart, "The ERA-Interim reanalysis: Configuration and performance of the data assimilation system," *Q. J. R. Meteorol. Soc.*, vol. 137, no. 656, pp. 553–597, Apr. 2011.

[14] G. S. Elsaesser and C. K. Kummerow, "Towards a fully parametric retrieval of the non-raining parameters over the global oceans," *J. Appl. Meteor. Climatol.*, vol. 47, no. 6, pp. 1599–1618, Jun. 2008.

[15] National Snow and Ice Data Center, Digital media National Ice Center Arctic Sea Ice Charts and Climatologies in Gridded Format, 2009, Digital media.

[16] R. W. Reynolds, T. M. Smith, C. Liu, D. B. Chelton, K. S. Casey, and M. G. Schlax, "Daily high-resolution blended analyses for sea surface temperature," *J. Climate*, vol. 20, no. 22, pp. 5473–5496, Nov. 2007.

[17] C. S. Ruf, "Detection of calibration drifts in spaceborne microwave radiometers using a vicarious cold reference," *IEEE Trans. Geosci. Remote Sens.*, vol. 38, no. 1, pp. 44–52, Jan. 2000.

[18] S. Brown and C. Ruf, "Determination of a hot blackbody reference target over the amazon rainforest for the on-orbit calibration of microwave radiometers," *J. Ocean. Atmos. Technol.*, vol. 22, no. 9, pp. 1340–1352, Sep. 2005.

[19] C. Prigent, E. Jaumouillé, F. Chevallier, and F. Aires, "A parameterization of the microwave land surface emissivity between 19 and 100 GHz, anchored to satellite-derived estimates," *IEEE Trans. Geosci. Remote Sens.*, vol. 46, no. 2, pp. 344–352, Feb. 2008.

[20] K. E. Trenberth, P. D. Jones, P. Ambenje, R. Bojariu, D. Easterling, A. Klein Tank, D. Parker, F. Rahimzadeh, J. A. Renwick, M. Rusticucci, B. Soden, and P. Zhai, *Observations: Surface and Atmospheric Climate Change. In: Climate Change 2007: The Physical Science Basis. Contribution of Working Group I to the Fourth Assessment Report of the Intergovernmental Panel on Climate Change*, S. Solomon, D. Qin, M. Manning, Z. Chen, M. Marquis, K. B. Averyt, M. Tignor, and H. L. Miller, Eds. Cambridge, U.K.: Cambridge Univ. Press.

Mathew R. P. Sapiano received the B.Sc. and M.Sc. degrees in statistics and Ph.D. degree in meteorology from the University of Reading, Berkshire, U.K., in 2000, 2001, and 2005, respectively.

Since 2012, he has been an Assistant Research Scientist at the Earth Systems Science Interdisciplinary Center at the University of Maryland, College Park. From 2009 to 2012, he was a Research Scientist in the Atmospheric Science Department at Colorado State University, Fort Collins.

Wesley K. Berg received the B.S., M.S., and Ph.D. degrees in aerospace engineering from the University of Colorado, Denver, in 1988, 1989, and 1993, respectively.

Currently, he is a Senior Research Scientist in the Department of Atmospheric Science at Colorado State University, Fort Collins. He worked previously at the Cooperative Institute for Research in Environmental Science within National Oceanic and Atmospheric Administration's Environmental Research Laboratories. His research interests involve satellite remote sensing of precipitation and other hydrologic parameters with a focus on the development and analysis of satellite retrievals for for climate applications.

Darren S. McKague received the Ph.D. degree in astrophysical, planetary, and atmospheric sciences from the University of Colorado, Boulder, in 2001.

He is an Assistant Research Scientist in the Department of Atmospheric, Oceanic, and Space Sciences at the University of Michigan, Ann Arbor. Prior to working for the University of Michigan, he worked as a Systems Engineer for Ball Aerospace and for Raytheon, and as a Research Scientist at Colorado State University, Fort Collins. His work has focused on remote sensing with emphases on the development of space-borne microwave remote sensing hardware, passive microwave calibration techniques, and on mathematical inversion techniques for geophysical retrievals. His experience with remote sensing hardware includes systems engineering for several advanced passive and active instrument concepts and the design of the calibration subsystem on the Global Precipitation Mission (GPM) Microwave Imager (MI) and the development of calibration techniques for the GPM constellation while at the University of Michigan. His algorithm experience includes the development of a near-real time algorithm for the joint retrieval of water vapor profiles, temperature profiles, cloud liquid water path, and surface emissivity for the Advanced Microwave Sounding Unit at Colorado State University, and the development of the precipitation rate, precipitation type, sea ice, and sea surface wind direction algorithms for the risk reduction phase of the Conical Scanning MI/Sounder.

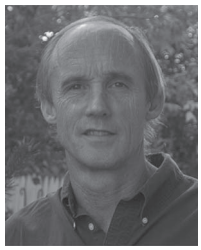

Christian D. Kummerow received the A.B. degree in physics from the University of California at Berkeley, Berkeley, in 1982, and the Ph.D. degree in atmospheric physics from the University of Minnesota, Minneapolis, in 1987.

Currently, he is a Professor in the Department of Atmospheric Science as well as the Director of the Cooperative Institute for Research in the Atmosphere at Colorado State University, Fort Collins. He served as Project Scientist for the Tropical Rainfall Measuring Mission (TRMM) between 1997 and 2000 and is currently the Chair of the GEWEX Data and Assessments Panel. His research interests focus on rainfall and its variability in the climate system. He has developed rainfall products from passive microwave sensors as well as combined active/passive methods. Understanding uncertainties in these estimates forms the basis of climate studies that seek to understand the sensitivity of precipitation to increased greenhouse gas concentrations. Significant research is therefore focused on precipitation as part of the Climate System with efforts focused on closing the water and energy budgets over not only global, but also regional scales.